

# The 'surf zone' in the stratosphere

M. E. MCINTYRE

Department of Applied Mathematics and Theoretical Physics, University of Cambridge,  
Cambridge CB3 9EW, U.K.

and

T. N. PALMER

Meteorological Office, Bracknell, Berks. RG12 2SZ, U.K.

(Received in final form 2 April 1984)

**Abstract**—Synoptic, coarse-grain, isentropic maps of Ertel's potential vorticity  $Q$  for the northern middle stratosphere, estimated using a large-Richardson-number approximation, are presented for a number of days in January–February 1979, together with some related isentropic trajectory calculations. The effects of substituting FGGE for NMC base data are noted, as well as some slight corrections to maps published earlier. The combined evidence from the observations and from dynamical models strongly indicates the existence of planetary-wave breaking, a process in which material contours are rapidly and irreversibly deformed. In the winter stratosphere this occurs most spectacularly in a gigantic 'nonlinear critical layer', or 'surf zone', which surrounds the main polar vortex, and which tends to erode the vortex when wave amplitudes become large. Some of the FGGE-based  $Q$  maps suggest that we may be seeing glimpses of local dynamical instabilities and vortex-rollup phenomena within breaking planetary waves. Related phenomena in the troposphere are discussed. An objective definition of the area  $A(t)$  of the main vortex, as it appears on isentropic  $Q$  maps, is proposed. A smoothed time series of daily values of  $A(t)$  should be a statistically powerful 'circulation index' for the state of the winter-time middle stratosphere, which avoids the loss of information incurred by Eulerian space and time averaging.

## 1. INTRODUCTION

In this Symposium and in a recent article in *Nature* (MCINTYRE and PALMER, 1983), we presented and discussed some synoptic maps of Ertel's potential vorticity  $Q$  on the 850 K isentropic surface, for the extratropical Northern hemisphere on several days during the warming events of January–February 1979. The 850 K isentropic surface lies in the middle stratosphere at altitudes around 30 km.  $Q$  is defined as

$$Q = \rho^{-1}(2\Omega + \nabla \times \mathbf{u}) \cdot \nabla \theta, \quad (1)$$

where  $\Omega$  is the Earth's angular velocity,  $\mathbf{u}$  is air velocity relative to the Earth,  $\rho$  is air density and  $\theta$  may be taken as specific entropy or any function of it, such as potential temperature. For a discussion of the approximations and data-processing procedures involved in constructing these isentropic  $Q$  maps, the reader is referred to the *Nature* article (hereafter MP) and to the Appendix A of this paper, and also to a forthcoming paper by CLOUGH *et al.* (1984).

The reason for thinking in terms of such maps, despite the well known difficulties in deriving them from real data, is that they are fundamentally the simplest and most useful way in which to visualize large-scale dynamical processes. This is not merely

because of the simplicity of the Lagrangian behaviour of  $Q$ , which is approximately a material tracer, but also because the distribution of  $Q$  controls the time development of almost every large-scale dynamical process of meteorological interest, through its diagnostic connection with the mutually balanced pressure and velocity fields. This important fact was implicitly recognized by V. Bjerknes in his early emphasis on the use of 'circulation theorems', following concepts originally developed by Kelvin and Helmholtz (GILL, 1982; PEDLOSKY, 1979). The point was made particularly clear by the work of CHARNEY and STERN (1962, equations 2.25b, 2.31); see also BRETHERTON (1966a) for the extension of the concept to include the lower boundary condition and HOSKINS *et al.* (1984) for its extension from quasi-geostrophic to semi-geostrophic theory and further refinements.

The most familiar dynamical uses of the potential vorticity concept refer to adiabatic processes like Rossby wave propagation, the Rossby-wave restoring effect being related to the isentropic *gradient* of  $Q$ , as is well known. However, frictional and diabatic effects need not be excluded from consideration. Indeed, an example in which we shall be interested is the way in which diabatic processes form the stratospheric circumpolar vortex each autumn. For some purposes

this, too, is simplest to think of directly in terms of the evolution of isentropic distributions of  $Q$ , rather than primarily in terms of the balanced wind, temperature and pressure fields and the ageostrophic circulations which couple them together.

The stratospheric  $Q$  maps presented in MP, being severely limited by data resolution and aliasing problems due *inter alia* to the spacing of satellite orbits (cf. SALBY, 1982, but also CLOUGH *et al.*, 1984), gave only a coarse-grained estimate of the large-scale  $Q$  distribution on one isentropic surface, "resembling a blurred view of reality seen through a pane of knobby glass". Despite this, our experience in working with these maps has been one of seeing what is happening in the stratosphere much more clearly than ever before. In particular, the maps gave the first reasonably convincing direct view of the breaking of planetary-scale Rossby waves, a phenomenon whose existence, and importance for large-scale dynamical and tracer-transport processes in the stratosphere, had been anticipated from theoretical and numerical modelling work, including the theory of nonlinear critical layers (e.g. STEWARTSON, 1978; WARN and WARN, 1978; MCINTYRE, 1982, and references therein; Fig. 2 below). The possibility of making this phenomenon directly visible, albeit in blurred and distorted form, arose from the enormous spatial scale of some of the wave-breaking events in the middle stratosphere. They span a large portion of the hemisphere and can almost certainly be called the 'world's largest' breaking waves.

The  $Q$  maps immediately suggested another key fact about the anatomy of large-scale dynamical and tracer-transport processes in the stratosphere, namely that in winter, especially late winter, the isentropic surfaces of the extratropical middle stratosphere are divided into two sharply-defined, zonally asymmetric regions, a polar *main vortex*, characterized by steep gradients of  $Q$  at its edge, surrounded by a broad *surf zone* within which systematic, large-scale gradients of  $Q$  are comparatively weak. As its name is meant to suggest, the surf zone appears to be the main region of wave breaking, where the strongest quasi-horizontal mixing and irreversible tracer transport takes place. It is a real-life analogue of the theoretical nonlinear critical layer. In the late winter of 1979 it occupied more than a third of the area of the entire northern hemisphere. We argued that this 'main vortex, surf zone' structure, and its observed time evolution, in which the surf zone broadened and the main vortex shrank as the winter progressed, can be attributed in large part to erosion of the main vortex by the action of the breaking planetary waves in the surf zone. Independent corroboration of this picture, and further details of it, including a clearer view of the equatorward boundary of the surf zone,

have emerged from recent analyses of LIMS ozone data from the Nimbus 7 satellite (LEOVY *et al.*, 1984). The results have thrown new light on phenomena such as stratospheric sudden warmings, and have important implications for modelling the transport of pollutants in the ozone layer.

In this paper we present a fuller account of the original evidence for the surf-zone concept, including some isentropic trajectory calculations whose results were described qualitatively in MP but not presented for lack of space. We also give some further discussion of the implications of that evidence not only for the middle atmosphere, but also for analogous, weather-related phenomena in the troposphere, which have long been familiar to synoptic meteorologists but which can now be seen in a new and simpler light. Both the stratospheric and the tropospheric cases seem to involve a basically similar interplay between wave generation, propagation and breaking, which is proving to be an important part of the highly inhomogeneous "wave-turbulence jigsaw puzzle" which must be pieced together if we are to improve our understanding of large-scale atmospheric flows, and our ability to predict them.

We also take the opportunity to present some further information about the stratospheric  $Q$  maps, acquired since the publication of the earlier (*Nature*) article particularly the extent to which the maps are affected by substituting FGGE\* for the original NMC† base analyses at 100 mbar while keeping the same stratospheric thickness estimates as before (from the Tiros-N Stratospheric Sounding Unit, hereafter SSU—see PICK and BROWNSCOMBE, 1981). In fact all the  $Q$  maps presented in this paper are FGGE-based, except those in Fig. 1. It seems reasonable to assume that the FGGE 100 mbar analyses are better on the whole than the NMC analyses, especially in the subtropics. The FGGE-based  $Q$  maps appear to show a little more detail about the nature of the wave-breaking process. In addition, we draw attention to a mistake in the computer code which produced the original, NMC-based  $Q$  maps, which regrettably was discovered after the original publication, MP, appeared in print. It does not affect the conclusions, having little effect on the qualitative features of interest, but it does, for instance, imply that for quantitative purposes the indicated maximum value  $Q_{\max}$  of  $Q$  in the main vortex was overestimated in the original maps (lying nearer the value given by the geostrophic approximation, instead

\* First GARP Global Experiment data, as analyzed at the European Centre for Medium Range Weather Forecasts.

† National Meteorological Center, Washington, DC.

of being given, as intended, by the gradient-wind approximation).

To illustrate the extent of the change, Fig. 1a presents the original, slightly incorrect, NMC-based  $Q$  map for 27 January 1979, some of whose qualitative features were emphasised in the discussion presented in MP, including the long tongue of high- $Q$  air, shown lightly shaded, which extends around the Aleutian anticyclonic vortex (Fig. 1c), and which was taken to be one of the more spectacular visible manifestations of wave breaking. The main vortex, as we defined it, is approximately the heavily shaded region. We identified most of the remaining area as belonging to the surf zone. Fig. 1b is the same map with the coding error corrected, so that the resulting changes can readily be seen. The qualitative features of interest are much the same in both these maps, but the highest contour value in the correct map (Fig. 1b) corresponds to 1.84 rather than 2.46 times the maximum planetary vorticity  $2\Omega$ , in terms of the convention used in MP and in equation (A4) below, with  $29\text{K mbar}^{-1}$  taken as the reference static stability. The situation is much the same in the case of the other maps. Figure 1c is the NMC-based 10 mbar height map for the same day.

## 2. WAVE BREAKING AND IRREVERSIBILITY

Before going further, it is necessary to say more precisely what we mean by wave breaking. Like the familiar breaking of surface gravity waves as they approach an ocean beach, the breaking of planetary or Rossby waves, as we conceive it, is characterized by a rapid and irreversible deformation of material contours. MP argued from wave-mean interaction theory that this is the most useful and fundamental sense in which the notion of wave-breaking can be generalized, from familiar instances, so as to cover all kinds of transverse (non-acoustic) wave motions in fluid media, including internal gravity waves and Rossby waves. It is whether or not the waves break, in the sense envisaged, that often dominates how effective they are at inducing quasi-permanent changes in the basic state on which they propagate, for instance in the distributions of angular momentum and of advected scalars.

The relevant material contours, for this purpose, are those which, under the conditions assumed by linear, nondissipative wave theory, would *not* deform irreversibly, but merely undulate back and forth\* (cf. the perceptive remarks by DICKINSON, 1969, p. 78). In the case of Rossby waves, which in nondissipative wave theory satisfy the relations

$$D\theta/Dt = 0 \quad (2)$$

\* - such undulations usually resulting from the restoring effect giving rise to the wave propagation (associated with the basic-state vertical density gradient in the case of gravity waves, and with the basic-state isentropic gradient of potential vorticity in the case of Rossby waves). For further discussion see PAGEOPH 123, 964-975. (1985)

and

$$DQ/Dt = 0, \quad (3)$$

where  $D/Dt$  is the material derivative, the relevant contours are the contours of constant  $Q$  in each isentropic surface, which are indeed material contours if equations (2) and (3) hold. Thus the breaking of Rossby waves, in the sense envisaged, should in principle be visible in  $Q$  maps. Taken at face value, Fig. 1 seems to be a case where this was also true in practice. The gross shape of the  $Q$  contour marked '4', enclosing the lightly shaded area, is roughly but strikingly suggestive of the material contour deformation expected theoretically for the simplest kind of Rossby wave-breaking event. A theoretical example, taken from the theory of barotropic, nonlinear critical layers in a dissipationless fluid, is shown in Fig. 2 (see caption for details). This represents an analytical solution, with infinitely good spatial resolution. The family resemblance to the phenomenon suggested by Fig. 1 is emphasised by means of the shading. The kinematics of such contour deformations involves the formation of thin tongues of advected material, which tend to become ever longer and thinner, an irreversible process for all practical purposes (see below) and, incidentally, illustrative of the physical reality behind the so-called potential-*enstrophy* 'cascade' (e.g. WELANDER, 1955; BATCHELOR, 1969; BRETHERTON and HAIDVOGEL, 1976; RHINES, 1979).

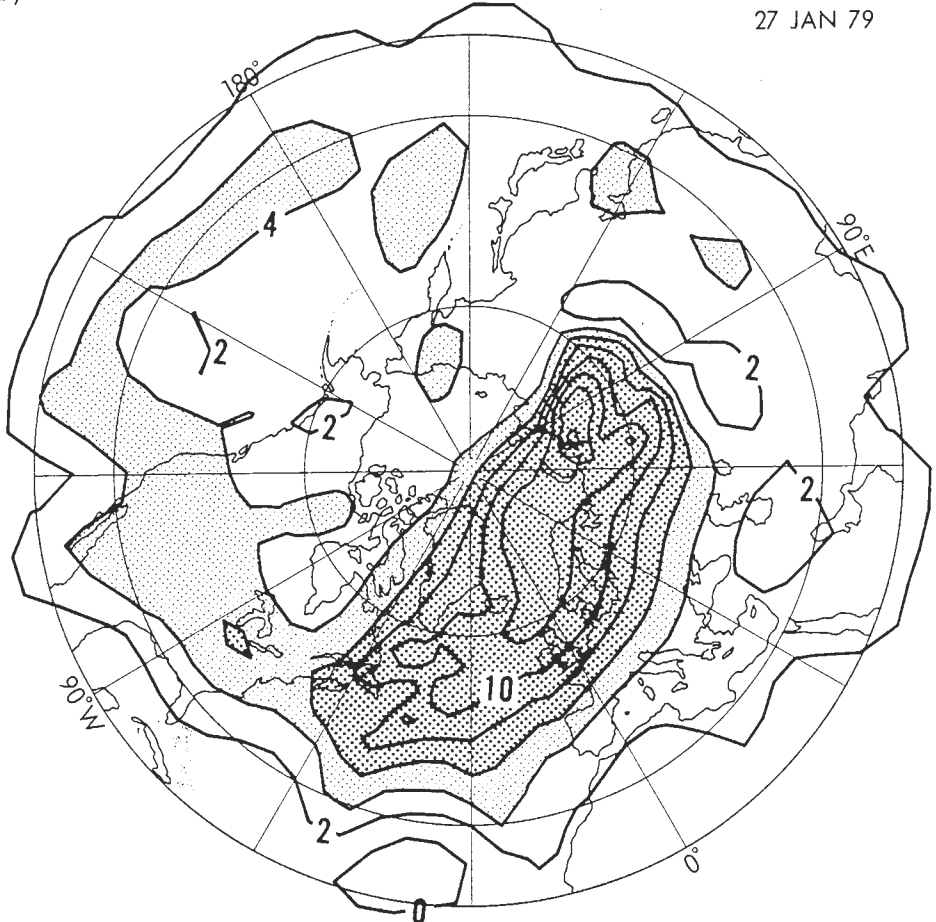
It should be borne in mind that such tongues, because of their tendency to become longer and thinner as time goes on, may rapidly disappear from view in any approximate representation having limited horizontal resolution, even if they involve a substantial isentropic contrast in  $Q$  values. An excellent illustration of this point can be seen in the numerical simulations of two-dimensional turbulence at different resolutions shown in Fig. 8a, b of HERRING *et al.* (1974).<sup>†</sup> Such tongues may also be dynamically unstable (the more so, the greater the contrast in  $Q$  values), because of the change in the sign of the isentropic gradient of  $Q$  across the tongue (CHARNEY and STERN, 1962). Although Charney and Stern studied only zonally symmetric flows, we have in mind a local approximation in which the narrowness of the tongue in comparison with its length permits it to be treated locally as if it were part of a zonally symmetric flow. Such instabilities might be capable of causing a tongue to break up into eddies at some stage of its evolution. The analytical solution of Fig. 2 has, in fact, been shown to be unstable in this way (KILLWORTH and MCINTYRE, 1984; HAYNES, 1984), but we are not yet sure how significant this might be for cases like that of Fig. 1, since the parameter regime is very different.

Whether or not such instabilities turn out to be

<sup>†</sup> See also the numerical "contour-dynamics" simulations reported in, for instance, Deem, G.S. and Zabusky, N.J. (1978) *Phys. Rev. Lett.* **40**, 859-862; Dritschel, D.G. (1987) *J. Fluid Mech.*, **172**, 157-182 (E.g. figure 13).

a)

NMC  
27 JAN 79



b)

NMC CORRECTED  
27 JAN 79

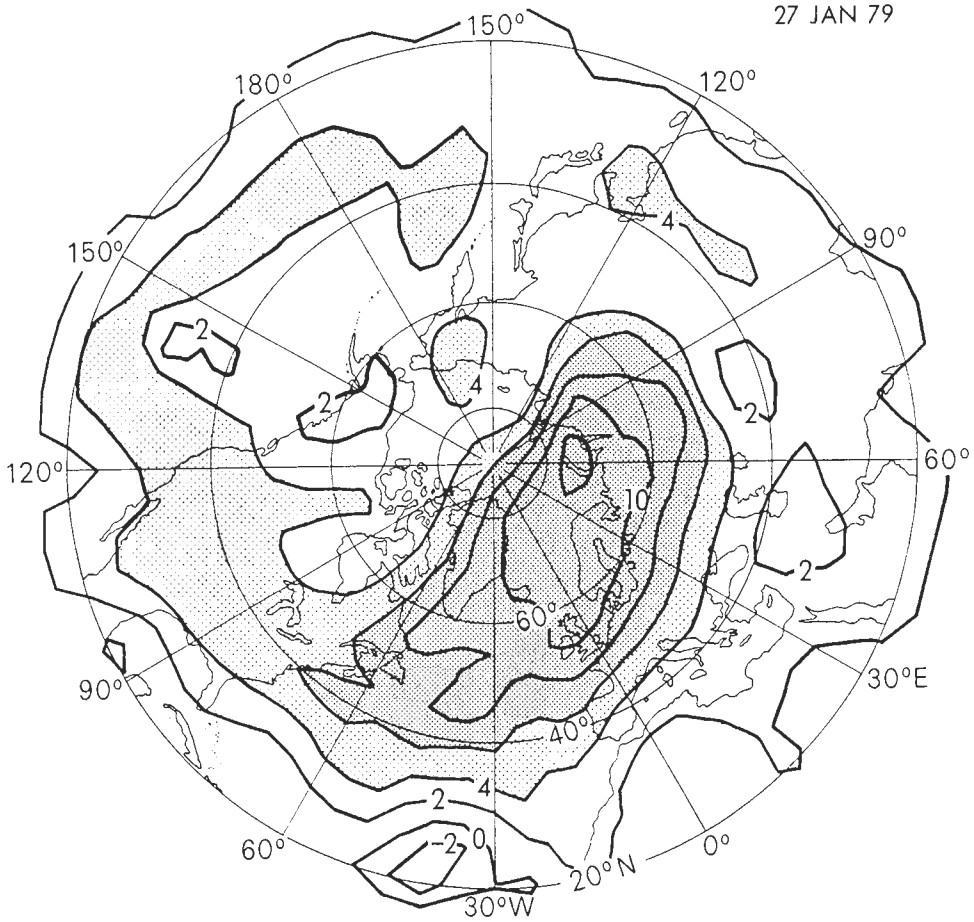


Fig. 1a, b  
(see over)

c)

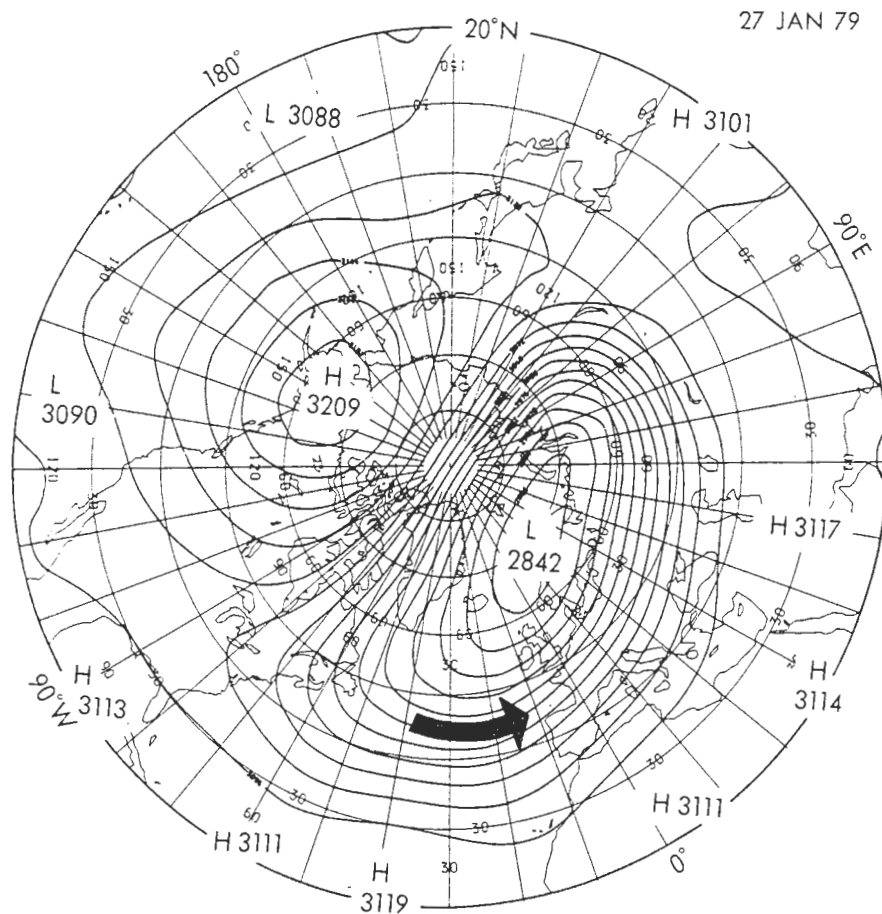


Fig. 1. (a), (b) Uncorrected and corrected coarse-grain NMC-based estimates of Ertel's potential vorticity  $Q$  (see text) on the 850 K isentropic surface, near the 10 mbar isobaric surface, on 27 January 1979 at 00Z. For units see Appendix A. Contour interval is 2 units. Values greater than 4 units are lightly shaded and greater than 6 units heavily shaded. (c) Corresponding NMC-based analysis of the geopotential height of the 10 mbar isobaric surface in dekametres. Contour interval is 24 dekametres. The lowest contour value is 28.56 km and the highest 31.92 km. Map projections are polar stereographic. The southernmost latitude circle shown is 20°N.

important, the length of time for which a wave breaking event can be followed in detail, if it is visible at all, will clearly be sensitive to the spatial scale of the event in relation to the horizontal resolution of the maps, as well as to the strength of the isentropic  $Q$  contrast across the tongue. Figure 1 corresponds to the wave event of largest amplitude and scale during the whole winter of 1978–79, and could well be a case where breaking was visible to an unusual extent despite the limited resolution. Caution should still be exercised, however, regarding the realism or otherwise of some details in the picture, especially near the far end of the tongue, which lies in the subtropical Pacific where the data quality may be worst. These questions will be taken up again in the next two sections.

Although the meaning of 'rapid and irreversible' deformation of material contours may seem almost self-

evident as soon as one has some specific examples in mind, including the familiar one of surface gravity waves on an ocean beach, it may be useful to be more specific. The rest of this section, and Appendix B, examines more closely what is involved.

Take 'rapid' first. A reasonable judgement as to what should be meant in general by rapid seems to be that the time scale of the material deformation should not be much longer than a typical intrinsic wave period in the locality concerned, and should also be much shorter than dissipative time scales. Slower, overtly dissipative processes can also lead to irreversible material deformation, through their cumulative effects over many wave periods, but it would not be natural to call this wave breaking. The analytical example of Fig. 2 is an example of rapid deformation in the foregoing sense. From the solution given in STEWARTSON (1978), it can

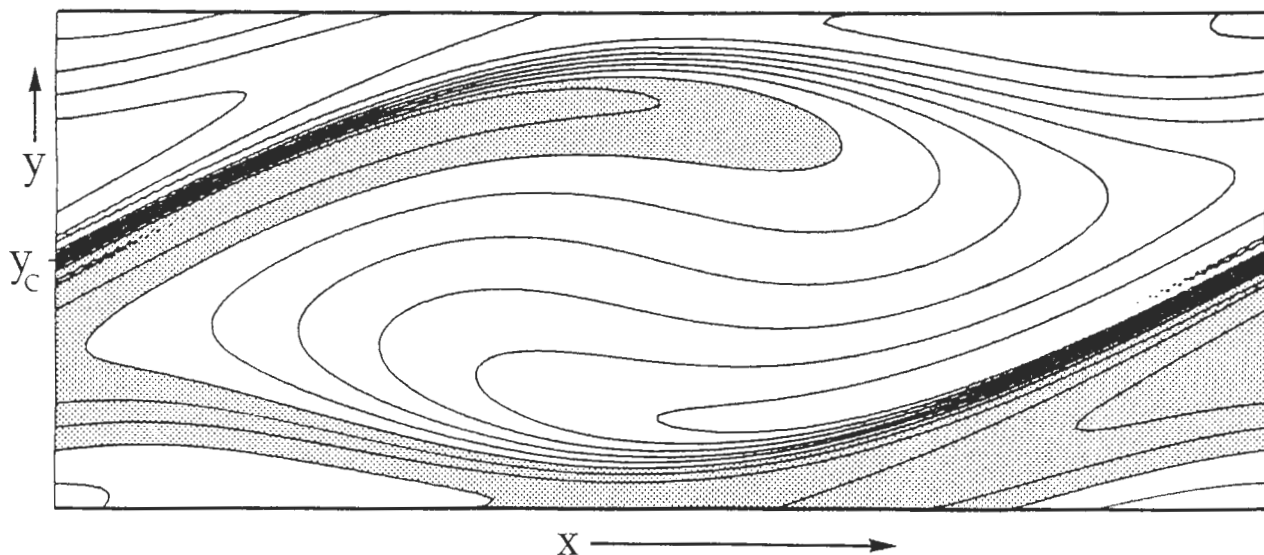


Fig. 2. Analytical solution from the theory of nonlinear critical layers (STEWARTSON, 1978; WARN and WARN, 1978), exhibiting the effectively irreversible deformation of material contours due to a two-dimensional (height-independent) 'Aleutian vortex' set up by a stationary Rossby wave on a shear flow. An equation of the form (3) holds exactly, and so the contours are both material contours and contours of  $Q$ , or equally (in this case) its two-dimensional counterpart, the vertical component of absolute vorticity. The shading picks out values of  $Q$  intermediate between the higher and lower values (unshaded) at bottom and at top/centre, respectively. The solution is periodic in  $x$ , which corresponds to longitude west for the purpose of a qualitative comparison with Fig. 1b. The  $y$  scale is exaggerated and corresponds to minus the latitude. Initially the contours lie parallel to the  $x$  axis. The initial flow is in the  $x$  direction, its velocity proportional to  $(y - y_c)$  so that there is a 'critical line' at  $y = y_c$ . The time elapsed is 0.57 of the time for an air parcel to make one complete trip around the centre of the vortex or 'cat's eye'. The solution can be shown to apply whether or not the contours represent equally spaced values of  $Q$ , i.e. it applies when the initial  $Q$  distribution is a given, arbitrary function of  $y$ . For instance the initial gradient could be small outside the shaded region.

be shown that the time for a material contour near the centre of the picture to rotate clockwise through  $360^\circ$  is just one intrinsic wave period, when the intrinsic wave period is evaluated from linear theory at a value of  $y$  halfway between the centre and the edge of the model 'Aleutian vortex', or slightly less than halfway between the centre and bottom of the picture.

Second, what do we mean by 'irreversible'? The notion of irreversibility in use here is similar, at a *conceptual* level, to that employed in ordinary statistical mechanics (for a clear discussion see PEIERLS, 1979, pp. 76, 79). But it should be kept firmly in mind that the associated physical phenomena, such as the continual lengthening of material contours and the accompanying potential-*enstrophy* 'cascade', are very different. These phenomena are to be carefully distinguished from phenomena associated with irreversibility of the microscopic, molecular and radiative processes usually studied in statistical mechanics, a quite separate set of phenomena also present in the real atmosphere. The mechanics we are concerned with here is that of the bulk fluid motion (particularly the large-scale, quasi-two-dimensional

fluid motion), not that of the individual air molecules and photons. The irreversibility in question would be present even in a fluid-dynamical model which, like the model from which Fig. 2 was obtained, had no overtly dissipative terms in its equations of motion, i.e. which utterly neglected the irreversibility due to microscopic processes. (Whether there exists a numerical method which could in any sense cope with such a model is an entirely separate question, to which the answer is no; but that does not destroy the legitimacy of the thought-experiments, and the resulting concepts, arising from a consideration of such models and their analytical solutions. The same can be said about the question of whether such models exhibit true statistical-mechanical *equilibria*—to which the answer is, again, almost certainly no. All we are concerned with here is the fact, for which the theoretical and empirical evidence is overwhelming, that they exhibit irreversibility. As is well known, this in no way contradicts the fact that the model equations are time-symmetric; see Appendix B.)

Figure 3, taken from WELANDER (1955), reminds us very effectively of the general nature of the fluid-

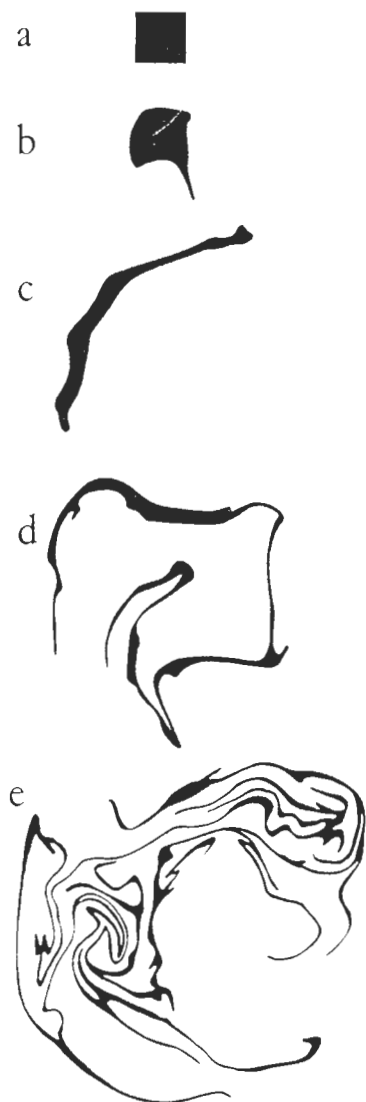


Fig. 3. A classical illustration of fluid-dynamical irreversibility (see text): deformation of a material contour marked by a passive tracer in a time-dependent, two-dimensional, approximately nondivergent velocity field. Time goes forward from (a) to (e). From WELANDER (1955).

dynamical irreversibility of interest here. It shows the evolution of a passive material tracer in a time-dependent, approximately two-dimensional velocity field, produced in a laboratory tank of water on a rotating table. Part of the fluid is marked with dye at a given instant (Fig. 3a) and then followed for subsequent times (Figs. 3b–e). A reversed evolution from (e) to (a) is never observed in practice, even though overt diffusion of dye plays no significant role. Notice the tendency for ever smaller scales to appear.

A similar, albeit not identical, behaviour has been found from numerical 'two-dimensional turbulence' experiments to be characteristic of the smaller scales in the  $Q$  distribution, when overt dissipation is small enough (e.g. HERRING *et al.*, 1974; BRETHERTON

and HAIDVOGEL, 1976; RHINES, 1979; HOLLOWAY and KRISTMANNSSON, 1984). This is to be expected since, although  $Q$  is not a passive tracer—a fact which is crucial to the Rossby restoring mechanism and hence, for instance, to the resistance to erosion of a *large-scale*  $Q$ -feature like the stratospheric main vortex— $Q$  nevertheless behaves somewhat like a passive tracer on sufficiently small scales. The mathematical reason lies in the smoothing properties of the operators for finding diagnostically the balanced height and velocity fields corresponding to given isentropic  $Q$  distributions (and a given mass distribution of  $\theta$ ). The operator giving the height field has the approximate character of an inverse Laplacian (CHARNEY and STERN, 1962, equation 2.25b; HOSKINS *et al.*, 1984), a fact correctly suggested by the smoothness of Fig. 1c in comparison with Fig. 1b. The operator giving the velocity field is the same followed by only a single spatial differentiation. Consequently, the velocity field tends to become insensitive to the ever-decreasing scales in the isentropic  $Q$  distributions, once a situation locally resembling that in Fig. 3e develops for whatever reason. In such situations, a rapidly varying, small-scale  $Q$  field is advected by a smoother, larger-scale velocity field, the two being only weakly correlated on small scales. Figure 2 is actually an extreme example of this scale effect, in that the small-scale correlation is weak enough to be exploited mathematically, permitting the use of the method of matched asymptotic expansions to derive the solution (STEWARTSON, 1978; WARN and WARN, 1978).

Another way of viewing the scale effect is to note that it corresponds to the well known weakening of the Rossby wave restoring mechanism as spatial scales become smaller. As smaller and smaller scales develop in the shape of a  $Q$  contour, the restoring mechanism, which depends on the correlation between the velocity and  $Q$  fields, becomes less and less capable of opposing the deformation of the contour. What is more, even if  $Q$  is not quite passive on the smallest scales, i.e. even if a significant local Rossby restoring effect remains, then the likely result is to make the contour shape more convoluted, if anything, than it would be for a passive tracer. Once the  $Q$  contours have begun to fold over, the Rossby wave mechanism will tend to manifest itself, if at all, in the form of the dynamical instabilities mentioned earlier. This is because the folding implies sign changes in the local isentropic gradient of  $Q$ , on which the local Rossby restoring mechanism depends. As is well known, the possibility of such dynamical instabilities, whether barotropic, baroclinic, or a mixture of the two, is related to the existence of oppositely-directed Rossby wave propagation in horizontally or vertically adjacent regions (FJØRTOFT, 1950; LIGHTHILL, 1963, p. 93; BRETHERTON, 1966b).<sup>†</sup> An example amenable to

analytical solution is again given by the special case of Fig. 2, where the instability analysis mentioned earlier provides us with a detailed picture. The upshot is that, in one way or another, the small-scale deformation of material contours coincident with contours of the  $Q$  distribution can be expected to be no less irreversible than the passive-tracer behaviour illustrated in Fig. 3, once the deformation is initiated. How important the averaged, large-scale dynamical effects of that deformation may be is a separate question, of course, the answer to which will depend very much on the detailed circumstances. The same goes for the related question of how complete or incomplete is the consequent mixing of the  $Q$  distribution.

Whether the word 'dissipation' should be used to refer to the effects of the fluid-dynamical irreversibility under discussion is philosophically a moot point. However, in a practical sense these quasi-two-dimensional fluid motions are, in effect, dissipative, and in a way that depends hardly at all on the presence or absence of small, overtly dissipative terms in the equations, provided that such dissipative terms only smear out the finest details in the  $Q$  field and have a correspondingly small effect on the velocity field. In formulating numerical models, the distinction between fluid-dynamical and molecular or radiative irreversibility tends to get blurred, of course, since all irreversible processes have to be lumped willy-nilly into artificial, overtly dissipative terms in order for the model equations to be tractable numerically at finite resolution. (The question then becomes how to choose the form of those terms so as to do the least damage to the basic processes being modelled, including the quasi-two-dimensional fluid-dynamical irreversibility.)

Finally, it is re-emphasised that the general concept of wave breaking, as developed here, in no way depends on the extent to which recognizable instabilities can be said to play a role in deforming the material contours. Instabilities are important in certain cases, but the crucial question, which is relevant to all cases, is whether or not the contour deformations are irreversible. Such deformations can take place with or without the help of recognizable instabilities. Cases in which instabilities are recognizable and important include quasi-hydrostatic internal gravity waves (e.g. LINDZEN 1967, 1981; HODGES, 1967) and internal gravity waves on layered basic states (PHILLIPS, 1966; WOODS, 1968). Instabilities have been shown theoretically to be important in the special Rossby wave example of Fig. 2, as already mentioned (see especially HAYNES, 1984). But there are other instances, including classical cases of surface gravity waves, where the concept of 'instability' is peripheral or irrelevant to the concept of wave breaking (e.g. BENJAMIN and OLVER,\*

1982, p. 146). The analytical solution shown in Fig. 2, which represents an unstable situation in which the instabilities have been artificially suppressed, provides us with a dynamically consistent thought-experiment in which the material deformation is, nonetheless, effectively irreversible (and destroys the initial large-scale gradient of  $Q$ ), without the help of any instabilities. As for the tongues of high- $Q$  air which we believe must be eroded from time to time into the real stratospheric surfzone, whether they are sufficiently unstable to make a major difference to what happens in the stratosphere is still an open question, although we shall see in Section 4 that there is now some direct evidence pointing towards the actual occurrence of such instabilities. It appears moreover that their effect may be to make the mixing less complete than might otherwise be the case.

### 3. AIR PARCEL TRAJECTORIES AND WAVE-BREAKING SIGNATURES

As mentioned in the last section, and in MCINTYRE and PALMER (1983), and as we shall also see from the FGGE-based  $Q$  maps, there is some doubt as to whether the data should really be showing us a tongue fully as long as that appearing in Fig. 1. Although the gross shape of the apparent tongue is extremely plausible by comparison with the simplest available theoretical models, we cannot be certain of the precise extent and strength of the real tongue, especially since the quality of the NMC base data, in particular, is probably approaching its worst in the subtropical Pacific. We therefore decided to see first of all whether isentropic trajectory calculations could throw any light on the matter. Such calculations have their own problems but at least they involve a certain amount of integration as well as differentiation, somewhat mollifying the effects of noise in the data.

Figure 4 shows a computer-generated plot of three bundles of isentropic trajectories, integrated backwards from three sets of positions centred on the 32.5°N latitude circle, within or near the apparent tongue of 27 January 1979. These were kindly produced for us by Mr J. Austin, using FGGE-based SSU gradient-wind fields computed on the 850 K isentropic surface (for details of the method see AUSTIN and TUCK, 1984). The small circles are time markers for each tenth of a day. If equation (2) were exactly satisfied, then the isentropic trajectories would represent the paths of material parcels, apart from effects due to the errors in the wind fields. The latter include not only data errors and space-time interpolation errors, but also errors from the finite differencing scheme used to estimate the gradient winds from the height fields, probably worst near the pole, since a latitude-longitude grid was used.

\* Also, e.g.: Longuet-Higgins & Cokelet 1976, Proc. Roy. Soc. London A 350, p. 17  
 Baker, Meiron & Orszag 1982, J. Fluid Mech. 123, p. 477  
 New 1983, J. Fluid Mech. 130, p. 219.  
 Pullin 1982, J. Fluid Mech. 119, 507 (517).  
 New, McIver & Peregine, J. Fluid Mech. 150, p. 244, 248.

An interesting discussion relevant to this is in Lindzen & West JAS 41, 3021.

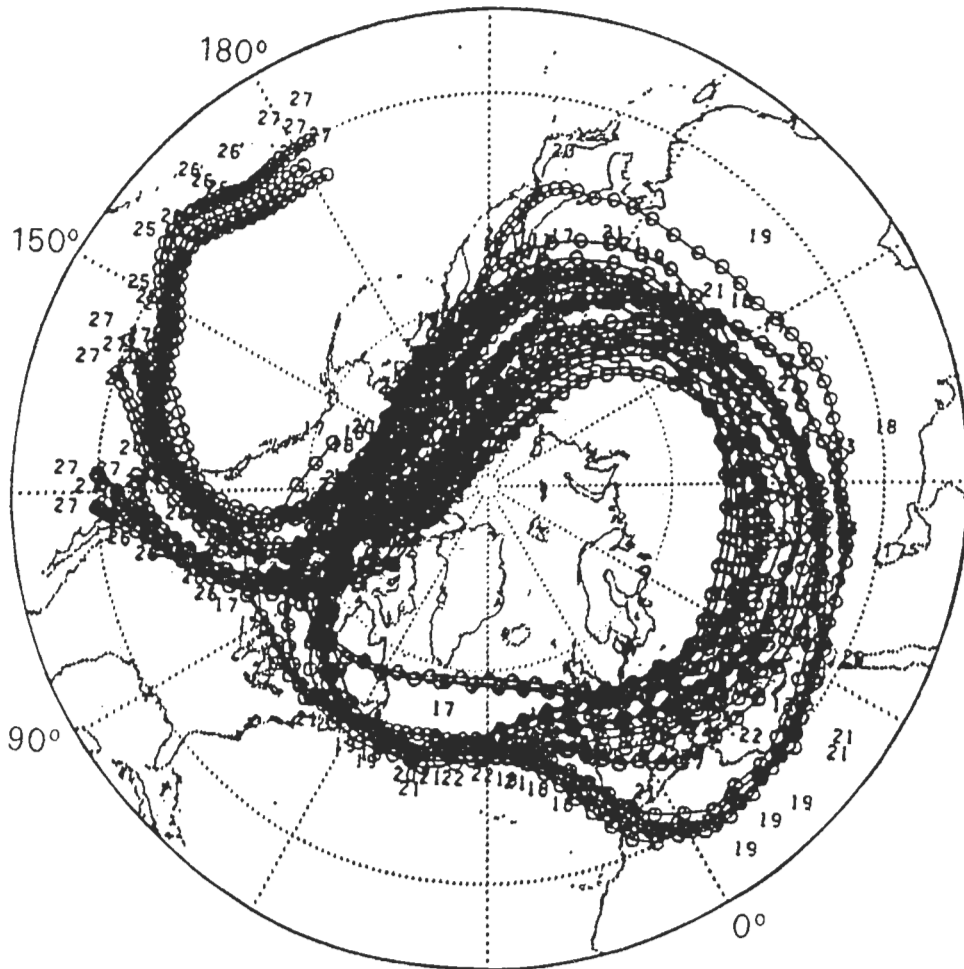


Fig. 4. Three bundles of machine-calculated 850 K isentropic trajectories ending on 27 January 1979. Time markers are shown every tenth of a day. Gradient winds were estimated from the Montgomery streamfunction on a latitude-longitude grid (see AUSTIN and TUCK, 1984) and the deceleration correction (A5) was applied. Dates shown by the computer graphics are at time 00Z.

A 'deceleration correction' was applied to allow for the error in the gradient-wind approximation itself, due to changes in the wind speed  $|\mathbf{u}|$  along the trajectory. That correction, described in Appendix A, can be cumulatively quite significant for an air parcel which peels off the rapidly-moving edge of the main vortex. The correction arises from the well known fact, neglected in the gradient-wind approximation, that an air parcel has to head slightly 'uphill', or more precisely, into the isobaric height gradient, if it is to reduce its speed (e.g. PALMÉN and NEWTON, 1969, §8.2).

Figure 5 gives an idea of the sensitivity of the trajectory calculations to the deceleration correction, and also to the choice of spatial differencing scheme from which to estimate the gradient winds. Four different estimates are shown for the part of the isentropic trajectory beginning on 23 January and ending at 177.5°W, 35°N on 27 January, with time markers every half day. The main scatter in the results is

between days 23 and 24, when the trajectories are emerging from the region of large horizontal wind shear near the edge of the main vortex.

The solid, heavy curve in Fig. 5 is the result of a hand computation ignoring the deceleration correction, done by careful graphical interpolation in space and time from machine-produced daily maps of FGGE-based SSU gradient-wind vectors. The gradient-wind vectors were computed from finite differences not on a latitude-longitude grid, but rather on a square grid on a polar stereographic projection, grid size about 580 km at 50°N, the same grid as was used for estimating  $Q$  (Appendix A). The heavy dotted curve shows the result of applying the deceleration correction from day 23 to 24, the main period of deceleration in this case, with  $|\mathbf{u}|$  going from 62 m s<sup>-1</sup> on day 23 up to a maximum of 72 m s<sup>-1</sup> and then steeply down to 34 m s<sup>-1</sup> on day 24. The correction brings the trajectory significantly nearer the pole. It would probably lie nearer still if the correc-

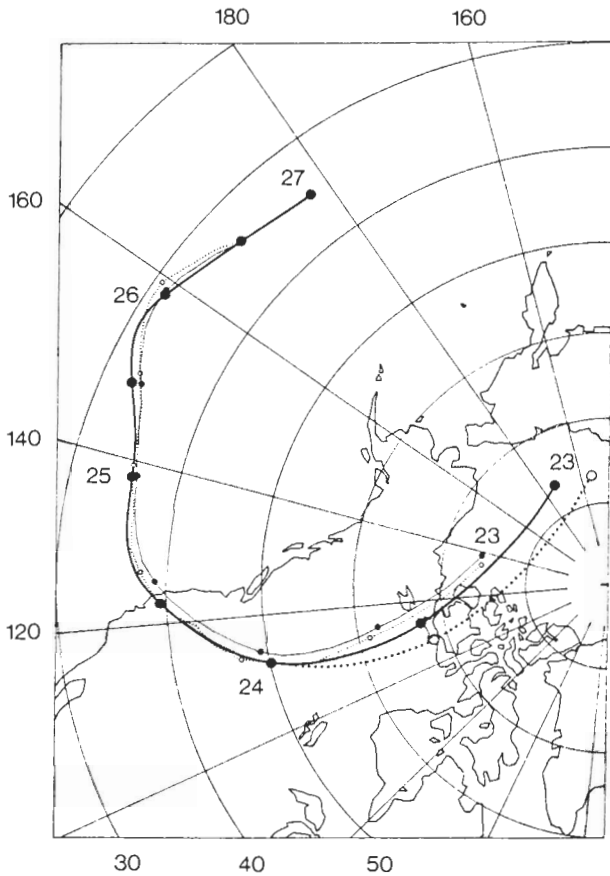


Fig. 5. Two hand-calculated (heavy curves) and two machine-calculated (light curves) 850 K isentropic trajectories, with time markers every half day, showing the effect of the deceleration correction (dotted curves with open time markers) and of different differencing schemes for computing the gradient wind (heavy versus light curves). See text.

tion had been applied instead from day 23 to 25, or over the whole trajectory, day 23 to 27, at the far end of which  $|\mathbf{u}|$  is down to about  $20 \text{ m s}^{-1}$ , but we did not attempt this because of uncertainty as to how to handle the effects of an unusually severe local nonuniformity in the estimated gradient-wind field encountered between days 24.5 and 25. This prevented us from applying the correction over that section with any real confidence that it would be meaningful, i.e. not strongly dependent upon particular choices of interpolation methods. The computational effects of this nonuniformity of the wind field upon the various differencing and interpolation schemes may well account for the larger scatter in the time markers for day 24.5, as compared to those for day 25 onwards, where the overall agreement with the light curves is remarkably good.

The light curves are two machine-calculated trajectories produced in the same way as for Fig. 4 using the gradient winds from the latitude–longitude grid. Points are plotted every tenth of a day and joined by

straight-line segments. The dotted curve reproduces the computation of Fig. 4, that is to say with the deceleration correction applied at each time step over the whole length of the trajectory. The time step was a hundredth of a day. The light, continuous curve is the corresponding machine computation without the deceleration correction. The cumulative effect of the deceleration correction can be seen to be much smaller in this case. This was traced to the fact that the gradient winds estimated from the latitude–longitude grid are considerably weaker than those from the polar stereographic grid in the computationally critical region near the edge of the main vortex. For instance, at day 23 on the corrected machine trajectory (beginning of the light dotted curve), the gradient-wind speed  $|\mathbf{u}|$  seen by the machine computation was only  $38.5 \text{ m s}^{-1}$ , as compared to about  $65 \text{ m s}^{-1}$  interpolated to the same point from the polar stereographic grid values from which the heavy curves in Fig. 5 were constructed. This accounts for the shorter length of the machine trajectories, as well as for the smaller deceleration correction.

Notice how the deceleration correction has a tendency to exacerbate the computational sensitivity near the edge of the main vortex. If  $|\mathbf{u}|$  at the beginning of a trajectory is large, then the acceleration correction is relatively large, bringing the trajectory further towards the pole and into still stronger winds, and so on. In the case of the heavy dotted curve in Fig. 5, it was found that one or two iterations were enough to settle its position at each time step. As already mentioned, the maximum value of  $|\mathbf{u}|$  on the heavy dotted curve was estimated to be  $72 \text{ m s}^{-1}$ . This occurred in the sector lying just north of  $80^\circ\text{N}$ . The maximum gradient-wind speed indicated on the polar stereographic grid for day 23 was  $82 \text{ m s}^{-1}$ , at  $84^\circ\text{N}$ ,  $126^\circ\text{W}$ .

The shape and position of the main vortex on day 23, defined in terms of the  $Q$  distribution on the 850 K isentropic surface, is indicated in Fig. 6, the FGGE-based  $Q$  map for 23 January. (Note that the contour interval is half that in Fig. 1). McINTYRE and PALMER (1983) defined the edge of the main vortex as the edge of the main region of steep  $Q$  gradients, which in the case of Fig. 6 can reasonably be placed somewhere within the lightly shaded, continuous band lying between the contour values 4 and 6. The edge of the main vortex, so defined, is very close to the starting points of the trajectories shown in Fig. 5. It is pointless to try to decide exactly how close, since, like the trajectories, the  $Q$  maps themselves are subject to finite-differencing errors on the polar-stereographic grid, as well as data errors. Moreover, diabatic corrections to the trajectories, and to equation (3) for the evolution of  $Q$  itself, have yet to be given a state-of-the-art assessment.

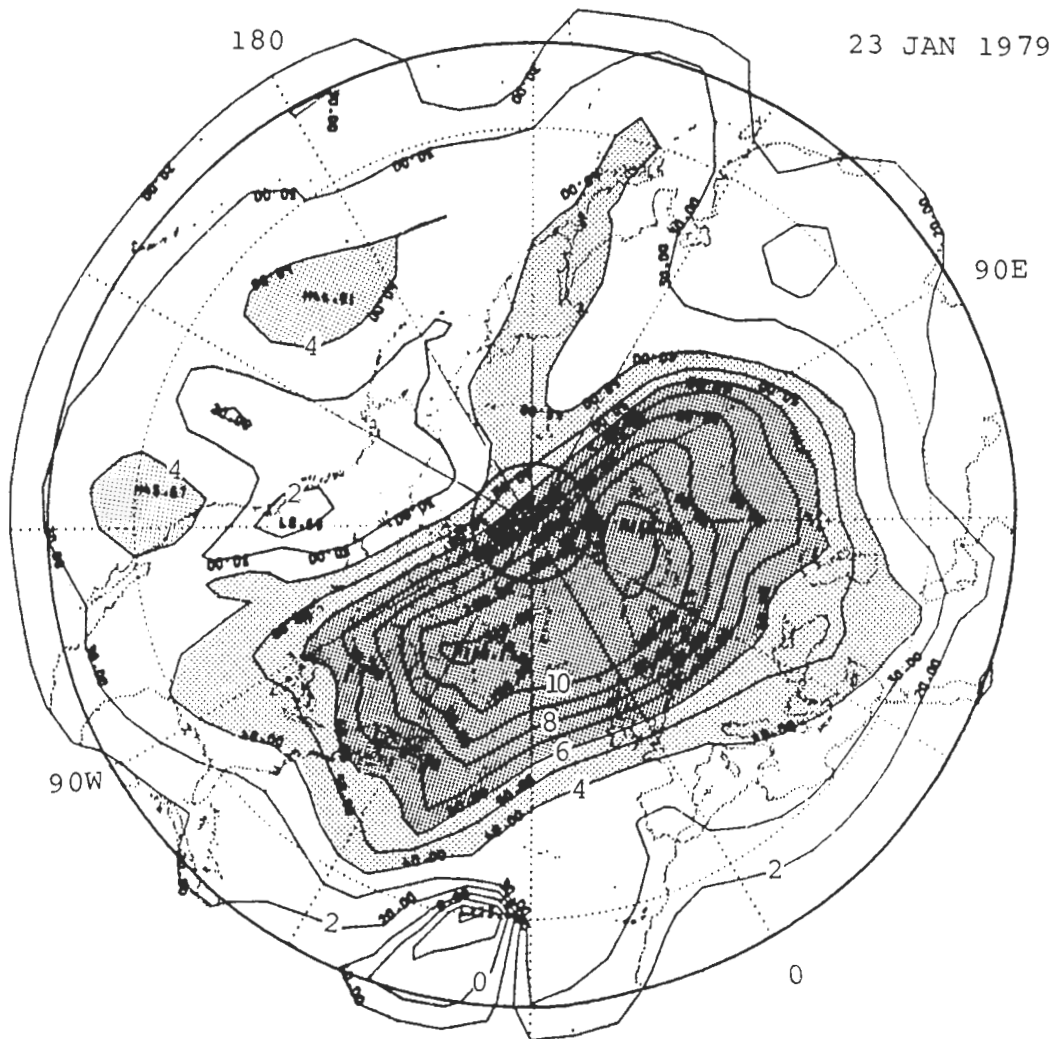


Fig. 6. Coarse-grain FGGE-based estimate of Ertel's potential vorticity on the 850 K isentropic surface on 23 January 1979 at 00Z (direct reproduction of the computer-generated plot). For units see Appendix A. Contour interval is 1 unit, twice as fine as in Figs. 1a, b. (The small computer-generated numbers are to be divided by 10, to give the units defined in Appendix A.) Values greater than 4 units are lightly shaded and those greater than 6 units heavily shaded, as in Figs. 1a, b. The 80°N latitude circle is shown (solid circle) in order to facilitate comparison with Fig. 5. Map projection is polar stereographic.

Among other things, this would require careful attention to the actual local distribution of ozone. However, it seems fair to say that all the evidence so far seems consistent, at least, with the general nature of the hypothesized wave-breaking and erosion mechanism, in which air parcels are removed from the edge of the main vortex and mixed quasi-horizontally into the surrounding surf zone, the whole process involving irreversible deformation of material contours.

It should be cautioned that the completeness or incompleteness of the mixing is not clear observationally; we cannot see the  $Q$  distribution in nearly enough detail to tell this directly. In addition, it should be kept in mind that other, overtly dissipative, processes may play a role in determining the fate of an air parcel eroded

from the main vortex. An important task for the future will be to assess this. For instance, if the vertical structure of the day-27 tongue were sufficiently baroclinic, then  $Q$  values in the tongue might be quite vulnerable to diabatically induced changes in the tropics. However, none of this argues against the likely physical reality and importance of the erosion mechanism itself.

The hypothesized picture becomes even more plausible when we take the circumstantial evidence into account, particularly the fact that the Aleutian vortex was in the process of growing towards its maximum size for the whole winter during the period in question, 23–27 January. On kinematical grounds alone this would appear to make erosion of the main vortex almost

